International Journal of Thermophysics (2023) 44:146
https://doi.org/10.1007/s10765-023-03250-x

Thermal Diffusivity and Fick Diffusion Coefficient in Mixtures of Hydrogen and Methane by Dynamic Light Scattering

Maximilian Piszko[1] · Patrick S. Schmidt[1] · Michael H. Rausch[1] · Andreas P. Fröba[1]

Received: 28 June 2023 / Accepted: 4 August 2023 / Published online: 12 September 2023

Abstract

Mixtures of hydrogen (H_2) and methane (CH_4) are given in many technical applications where accurate thermophysical property data are required for the design and optimization of corresponding processes. This work evaluates the accessibility of the thermal diffusivity a and the Fick diffusion coefficient D_{11} in gaseous binary mixtures of H_2 and CH_4 by dynamic light scattering (DLS). The investigations are performed at temperatures T and pressures p of (293, 333, 363, and 393) K and (5, 10, and 15) MPa with varying CH_4 mole fractions x_{CH_4} of (0.05, 0.3, 0.6, and 0.8). For all thermodynamic states investigated, only one hydrodynamic mode was observable by DLS. The assignment of the single related diffusivity to either a, D_{11}, or a mixed diffusivity D_{mix} representing both a and D_{11} is performed by considering D_{11} calculated by the Chapman–Enskog kinetic theory, experimental D_{11} literature data, a predicted by using two different approaches, and calculations of the so-called Rayleigh ratio. The findings indicate that DLS gives access to a at high x_{CH_4}, D_{11} at low x_{CH_4}, and D_{mix} at $x_{CH_4} \approx 0.3$. All data are summarized in the form of correlations providing a and D_{11} as a function of T, p, and x_{CH_4}.

Keywords Binary gas mixtures · Diffusivities · Dynamic light scattering · Hydrogen · Methane

Special Issue in Honor of Professor Roland Span's 60th Birthday.

✉ Andreas P. Fröba
andreas.p.froeba@fau.de

[1] Institute of Advanced Optical Technologies – Thermophysical Properties (AOT-TP), Department of Chemical and Biological Engineering (CBI) and Erlangen Graduate School in Advanced Optical Technologies (SAOT), Friedrich-Alexander-Universität Erlangen-Nürnberg (FAU), Paul-Gordan-Straβe 8, 91052 Erlangen, Germany

1 Introduction

Hydrogen (H_2) is currently discussed as a working fluid for energy storage and transport in connection with the expansion of renewable energies [1, 2]. Its large-scale utilization requires the development of technologies for H_2 production [3–6], distribution [7], and storage [8, 9]. There are many conventional technical processes involving mixtures of H_2 and methane (CH_4), e.g., the production of H_2 from natural gas by steam reforming [10] or pyrolysis [11] as well as the photocatalytic production of H_2 and CH_4 from glycerol reforming [12]. To advance the energy transition by promoting the use of H_2 preferably produced via renewable energy resources, the utilization of H_2-natural gas blends (HNGBs) seems to be a promising solution because the blended H_2 can be transported through existing natural gas pipelines that are not suitable for pure H_2 [13]. The advantage of HNGBs is the significantly higher energy storage capacity [14] compared to pure H_2 or CH_4 and the possibility of their storage in form of clathrate hydrates [15]. Furthermore, for the large-scale storage of H_2 produced, for example, from offshore wind energy, the use of depleted reservoirs or subsurface caverns is currently under discussion [16]. In such reservoirs, CH_4 might be a pre-existing residual or intentionally used as cushion gas [17–19].

In connection with mixtures of H_2 and natural gas or CH_4, Roland Span and coworkers have contributed to an improved understanding of equilibrium properties, for instance, by reporting (pressure p, density ρ, temperature T, composition x) data [20] as well as an equation of state (EoS) [21]. For the application of mixtures of H_2 and CH_4, further key properties necessary for the design and optimization of corresponding processes [22–24] are the viscosity η, the thermal diffusivity a or the thermal conductivity λ, and the Fick diffusion coefficient D_{11}, which allow the characterization of momentum, heat, and mass transfer. At present, corresponding experimental data for mixtures of H_2 and CH_4 at process- or storage-relevant conditions are scarce [25, 26] whereas many studies report on transport properties at atmospheric pressure [27–29].

As dynamic light scattering (DLS) has been shown to be a powerful tool for the accurate determination of a and D_{11} in binary fluid mixtures over a wide range of T and p, see, e.g., Refs. [30–32], it can be used to overcome this lack of data. With this method, transport properties are accessible in an absolute way by the temporal analysis of the scattered-light intensity that is modulated by microscopic fluctuations in T or entropy and in concentration in macroscopic thermodynamic equilibrium [33, 34]. While for binary liquid mixtures, two hydrodynamic modes related to a and D_{11} are simultaneously accessible in most cases, often only one hydrodynamic mode may be accessible by DLS experiments in binary gaseous mixtures [35, 36]. Reasons for this are a difficult separability of the two modes, since a and D_{11} do not differ by more than a factor of two in the gas phase for many mixtures, as well as the amplitude ratio of the signal contribution related to fluctuations in concentration to that corresponding to T fluctuations. Furthermore, taking into account the signal-to-noise ratio (SNR), each signal contribution must have a sufficiently large amplitude to be resolvable.

In this work, mixtures of H_2 and CH_4 with mole fractions x_{CH_4} of (0.0533, 0.3125, 0.6180, and 0.8319) as well as pure CH_4 are investigated at T of (293, 333, 363, and 393) K and p of (5, 10, and 15) MPa by DLS. The accessibility of a, D_{11}, or a mixed diffusivity D_m representing both is examined by considering D_{11} calculated by the Chapman-Enskog kinetic theory, experimental D_{11} literature data, a predicted by using two different approaches, and calculations of the so-called Rayleigh ratio $\mathfrak{R}$. The latter gives an indication of what kind of fluctuation dominates the observable signals in the DLS experiments.

In the following, relevant information on the theory of DLS as well as some details on the Chapman–Enskog theory, the methodologies for the prediction of a, and on the calculation of $\mathfrak{R}$ are given. In the experimental part, the samples used as well as the experimental conditions, data analysis, and signal assignment strategy are described. Then, the experimental results are presented and assigned to either a, D_{11}, or D_m and discussed in comparison with literature including theoretical calculations. Afterwards, all data are summarized in the form of correlations providing access to a and D_{11} as a function of T, p, and x_{CH_4}.

2 Theoretical Background

2.1 Rayleigh Scattering from the Bulk of Binary Fluid Mixtures

For a binary mixture in macroscopic thermodynamic equilibrium, the frequency-unshifted Rayleigh component of the characteristic broadened spectrum of the scattered light consists of two contributions governed by microscopic statistical fluctuations in T or entropy and species concentration [33, 34, 37]. The width of both contributions is related to a and D_{11} while the magnitudes of their amplitudes depend mainly on the so-called optical contrast factors, the osmotic compressibility, the isobaric heat capacity, and T [38, 39]. Since the broadening of the spectrum is too small to be resolved in the frequency domain, the analysis of the scattered light observable at a well-defined scattering vector

$$q = \frac{4\pi n}{\lambda_0} \sin\left(\frac{\Theta_S}{2}\right) \tag{1}$$

is performed in the time domain by calculating the second-order or intensity correlation function. In Eq. 1, Θ_S and n are the scattering angle and the refractive index of the fluid at the laser wavelength in vacuo λ_0. The normalized intensity correlation function (CF) related to the Rayleigh component and recorded in a heterodyne detection scheme, where much stronger reference light is coherently superimposed with the scattered light from the sample, takes the form

$$g^{(2)}(\tau) = b_0 + b_t \exp\left(-|\tau|/\tau_{C,t}\right) + b_c \exp\left(-|\tau|/\tau_{C,c}\right). \tag{2}$$

Here, b_0, b_t, and b_c are experimental constants defined by the characteristics of the optical setup, the thermodynamic state, and the strength of the local oscillator

field. The decay times $\tau_{C,t}$ and $\tau_{C,c}$, which are equivalent to the mean lifetimes of the observed microscopic T and concentration fluctuations, are related to a and D_{11} by

$$\tau_{C,t} = (aq^2)^{-1} \text{ and } \tau_{C,c} = (D_{11}q^2)^{-1}. \tag{3}$$

Whether two contributions related to fluctuations in T and concentration can be resolved experimentally depends on the following factors. A first indication is the Lewis number $Le = a \cdot {D_{11}}^{-1}$, which should be either larger than 1.5 or smaller than 0.5 to ensure that a sufficient temporal separation of the two modes is given. Furthermore, neither of the signal amplitudes associated with the fluctuations in T, b_t, and in concentration, b_c, should be very large or very small. In general, the closer the ratio $b_c \cdot {b_t}^{-1}$ is to unity, the larger the deviation of Le from unity should be to allow for a detection of both contributions.

For Le very close to unity, only one apparent diffusivity related to both transport properties, i.e. a and D_{11}, can be accessed. To be consistent with previous work [36], this diffusivity is denoted as mixed diffusivity D_m in the following. When Le is not very close to unity, e.g., for about $0.4 < Le < 0.9$ or $1.1 < Le < 1.6$, either two modes and, thus, a and D_{11} or only a single mode and, thus, D_m can be accessed. For the latter case, D_m represents a if $b_t \gg b_c$ or D_{11} when $b_c \gg b_t$. Here, the larger the differences in b_t and b_c, the better is the agreement between D_m and a or D_{11}. Furthermore, even if Le is far from unity, only a single mode might be accessible when either b_t or b_c tends to zero. The individual signal amplitudes b_t and b_c cannot be determined experimentally in an absolute way because of unknown experimental constants. However, $\mathfrak{R} = b_c \cdot {b_t}^{-1}$ is experimentally accessible—assuming that two hydrodynamic modes can be resolved—and can be calculated theoretically as detailed later. Knowledge of $\mathfrak{R}$ provides an indication of the type of fluctuation that dominates the experimental CFs when only one hydrodynamic mode is resolvable in the DLS experiment. For additional information on these aspects, the reader is referred to Ref. [36], where the accessibility of diffusivities in an equimolar mixture of CH_4 and propane is analyzed.

The situation becomes more complex when coupling between heat and mass transfer occurs, which would lead to the observation of effective diffusivities [39–42]. Due to the lack of reliable data for the osmotic compressibility and the Soret coefficient for the studied thermodynamic states, it was not possible to estimate the mode-coupling parameter. Nevertheless, the influence of coupling between heat and mass transfer can most likely be neglected since the present measurements are performed in the gas phase far from the plait critical point and since the Soret coefficient of mixtures of H_2 and CH_4 estimated from thermodiffusion constant data [43] is on the order of 1×10^{-3} K^{-1}.

2.2 Prediction of the Fick Diffusion Coefficient of Gaseous Mixtures

In this work, D_{11} was estimated as a function of T, p, and x_{CH_4} with the Chapman-Enskog kinetic theory [44] as thoroughly described in the work of Marrero and Mason [27]. The main intention of these calculations is the assignment of the experimentally determined values to the different diffusivities. Only the most relevant

details are given below. The aforementioned authors define the second approximation of the Fick diffusion coefficient $[D_{11}]_2$ as

$$[D_{11}]_2 = [D_{11}]_1(1 + \Delta_{12}), \tag{4}$$

where the composition-independent first approximation of the diffusion coefficient is given by

$$[D_{11}]_1 = \mathrm{A}\left(\frac{M_1 + M_2}{2M_1M_2}\right)^{1/2} \frac{T^{3/2}}{p_\mathrm{a}\overline{\Omega}^{(1,1)}_{12,\mathrm{mix}}} \tag{5}$$

and the temperature- and composition-dependent correction term takes the form

$$\Delta_{12} = -\frac{\left(6C^*_{12} - 5\right)^2}{10}\left(\frac{x_1^2P_1 + x_2^2P_2 + x_1x_2P_{12}}{x_1^2Q_1 + x_2^2Q_2 + x_1x_2Q_{12}}\right). \tag{6}$$

In Eq. 5, M_1 and M_2 are the molar masses in $\mathrm{g{\cdot}mol^{-1}}$, p_a is the pressure in atm, and $\overline{\Omega}^{(1,1)}_{12,\mathrm{mix}}$ is the diffusion collision integral related to the mixture in $\mathrm{Å}^2$. The constant A = 0.008 258 is reported by Marrero and Mason [27] and must have the units $\mathrm{cm^2{\cdot}g^{0.5}{\cdot}atm{\cdot}Å^2{\cdot}s^{-1}{\cdot}mol^{-0.5}{\cdot}K^{-1.5}}$ to obtain a diffusivity in $\mathrm{cm^2{\cdot}s^{-1}}$. In Eq. 6, P_1, P_2, P_{12}, Q_1, Q_2, and Q_{12} are defined by extensive algebraic expressions [27] and

$$C^*_{12} = \frac{\Omega^{(1,2)^*}}{\Omega^{(1,1)^*}} \tag{7}$$

is the ratio of the reduced collision integrals $\Omega^{(1,1)^*}$ and $\Omega^{(1,2)^*}$. These reduced collision integrals are generally tabulated as a function of the reduced temperature $T^* = T{\cdot}(\varepsilon/k_\mathrm{B})^{-1}$ [45], where ε is the energy parameter of the Lennard–Jones (LJ) potential, i.e., the potential well depth, and k_B is the Boltzmann constant. For the mixtures of H_2 and CH_4 with varying composition, ε/k_B of each mixture, $(\varepsilon/k_\mathrm{B})_\mathrm{mix}$, was obtained by the linear mixing rule

$$(\varepsilon/k_\mathrm{B})_\mathrm{mix} = x_1(\varepsilon/k_\mathrm{B})_1 + (1 - x_1)(\varepsilon/k_\mathrm{B})_2, \tag{8}$$

where $(\varepsilon/k_\mathrm{B})_1$ and $(\varepsilon/k_\mathrm{B})_2$ for the pure gases were taken from Ref. [46]. For each state point, the obtained $(\varepsilon/k_\mathrm{B})_\mathrm{mix}$ was used to calculate T^* in the same way as described for a pure substance before. Then, the values for the reduced collision integrals for the LJ 12-6 potential function used in Eq. 7 were taken for the nearest T^* tabulated. $\overline{\Omega}^{(1,1)}_{12,\mathrm{mix}}$ was accessed via

$$\overline{\Omega}^{(1,1)}_{12,mix} = \Omega^{(1,2)^*}\pi\sigma^2_\mathrm{mix} \tag{9}$$

with

$$\sigma_\mathrm{mix} = x_1\sigma_1 + (1 - x_1)\sigma_2. \tag{10}$$

In Eq. 10, the LJ parameters σ_1 and σ_2 for CH_4 and H_2 were taken from Ref. [46].

2.3 Prediction of the Thermal Diffusivity of Gaseous Mixtures

The thermal diffusivity of gaseous mixtures a_{mix} was predicted using a model proposed by Lima et al. [47]. This model was developed for gas mixtures consisting of carbon dioxide (CO_2) and air. The model was further validated in a follow-up study [48] examining binary mixtures of CO_2, nitrogen, CH_4, and ethylene. It has the form [47]

$$a_{mix} = a_2 \left(\frac{\beta^{x_1}}{\left[1 + (\chi - 1)x_1\right]} \right), \tag{11}$$

where the parameters β and χ are

$$\beta = \frac{\lambda_1}{\lambda_2} \tag{12}$$

and

$$\chi = \frac{\rho_1 c_{p,1}}{\rho_2 c_{p,2}}. \tag{13}$$

In Eqs. 11–13, the indices 1 and 2 distinguish the components 1 and 2. Furthermore, ρ, c_p, and λ denote the density, specific heat capacity at constant pressure, and thermal conductivity. For H_2, ρ and c_p were calculated by an equation of state (EoS) from Leachman et al. [49] and λ was obtained from a correlation reported by Assael et al. [50]. For CH_4, ρ and c_p were calculated by an EoS from Setzmann and Wagner [51] and λ was taken from Friend et al. [52]. a was obtained via the relationship $a = \lambda \cdot \rho^{-1} \cdot {c_p}^{-1}$ for both H_2 and CH_4. To preserve the predictive nature of Eq. 11, the a values of pure CH_4 determined in this work were not used as input parameter.

To allow further comparison, a_{mix} was also obtained by using the aforementioned pure property data and the mixing rule for CH_4 and H_2 by Kunz and Wagner [53, 54] as implemented in the REFPROP software [55]. For this, the mixture density ρ_{mix}, mixture specific heat capacity $c_{p,mix}$, and mixture thermal conductivity λ_{mix} are combined according to

$$a_{mix,REFPROP} = \frac{\lambda_{mix}}{\rho_{mix} c_{p,mix}}. \tag{14}$$

The index of a in Eq. 14 is chosen due to simplicity and used in the following.

2.4 Rayleigh Ratio Calculations

The Rayleigh ratio

$$\mathfrak{R} = \frac{b_c}{b_t} = \frac{c_p}{T}\left(\frac{\partial c}{\partial \mu}\right)\frac{\left(\frac{\partial n}{\partial c}\right)^2}{\left(\frac{\partial n}{\partial T}\right)^2}, \tag{15}$$

representing the ratio of the signal amplitude of fluctuations in concentration, b_c, to that related to the fluctuations in T, b_t, can be used to identify the observable hydrodynamic modes in a DLS experiment [39, 41]. In the present work, the procedure for the calculation of $\mathfrak{R}$ is almost identical to that described in Ref. [36]. The refractive index n was estimated using the Lorentz–Lorenz equation [56] combined with a linear mixing rule [57] applying a simple mass-weighting scheme. The optical contrast factors $(\partial n/\partial T)$ and $(\partial n/\partial c)$, where c is the mass fraction of the heavier component, were calculated using well-established analytical expressions [57–59]. For their evaluation, average molecular polarizabilities were taken from the Refs. [59, 60]. The mixture data ρ_{mix} and $c_{p,mix}$ were estimated as described in Sect. 2.3. The partial derivatives of ρ_{mix} required for the calculation of $(\partial n/\partial T)$ and $(\partial n/\partial c)$ were calculated by representing ρ_{mix} as a function of T and c by second-order polynomials. The estimation of the osmotic compressibility $(\partial c/\partial \mu)$ [36], where μ is the difference between the chemical potentials of the pure components in the mixture, showed discontinuities. Even though a continuous behavior for $(\partial c/\partial \mu)$ was obtained by using the approach of DuBois and Berge [61], the magnitude of $\mathfrak{R}$ could not be predicted reliably. This can be related to the relatively large influence of $(\partial c/\partial \mu)$ on $\mathfrak{R}$. For this reason, results for $\mathfrak{R}$ are not presented and discussed in detail in this work. Nevertheless, the qualitative behavior of $\mathfrak{R}$ as a function of T, p, and x_{CH_4} can be used to support the assignment of the observed hydrodynamic modes or diffusivity data.

3 Experimental Section

3.1 Materials

The sample mixtures investigated in the present work were provided by Linde GmbH premixed in gas cylinders with an initial p of about 18 MPa. The purities of H_2 (component 2) and CH_4 (component 1) used for the preparation of the mixtures and individual investigations were (0.999 999 and 0.999 995). The mixture compositions stated in the certificate of analysis provided by Linde GmbH are x_{CH_4} = (0.0533, 0.3125, 0.6180, and 0.8319) and their expanded uncertainty (coverage factor $k = 2$) is stated to be 0.01. The relatively high uncertainty in the mixture composition is due to a gravimetric preparation in cylinders of a volume of 2 l. All samples were used without further purification.

3.2 Experimental Setup and Conditions

In the following, a summary of the essential features of the setup as well as information about the sample handling and the measurement conditions will be given.

Figure 1 shows a sketch of the optical and electronic arrangement of the apparatus used in the present work. A continuous-wave laser operated at $\lambda_0 = 532$ nm is used for the generation of scattered light. The latter is analyzed under a well-defined scattering angle Θ_S, which is defined as angle between the detection direction of scattered light and the direction of the incident laser light in the sample fluid. Θ_S determines the modulus of the scattering vector q, see Eq. 1, and can be expressed as a function of the experimentally accessible incident angle Θ_I by the Snell–Descartes law of refraction

$$n_{\text{fluid}} \sin \Theta_S = n_{\text{air}} \sin \Theta_I \tag{16}$$

with $n_{\text{air}} \approx 1$. Θ_I is the angle difference between the scattering direction and the direction of the incident laser light outside the sample or measurement cell and is measured by an autocollimation method with an estimated expanded uncertainty ($k = 2$) of 0.01°. The detection direction of the scattered light is fixed by two apertures (A) placed behind the sample cell (SC) and in front of the detection unit, which consists of two photomultiplier tubes (PMTs) operated in a pseudo-cross-correlation scheme to suppress afterpulsing and dead-time effects. The pulses of the PMTs are discriminated, amplified, and fed to two different digital correlators [31]. In this work, a heterodyne detection scheme is applied. This can be realized by using either an external reference beam separated from the main beam by a beam splitter or by using the window flares. Combinations of lambda-half wave plates (λ/2) and polarization beam splitters (PBS) located in both the main and the reference beam paths are used to adjust intensity and polarization. An additional neutral density filter (ND) and a linear grey filter (GF) are inserted in the path of the reference beam for further intensity attenuation.

T of the sample cell was measured by an AC bridge and two Pt100 resistance probes calibrated with an absolute expanded uncertainty ($k = 2$) of 15 mK. The

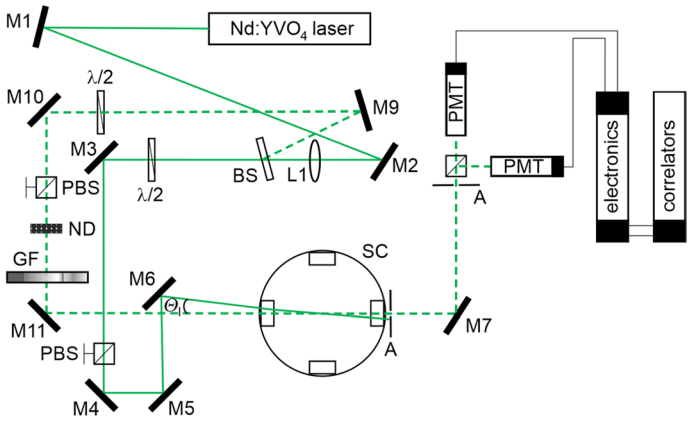

Fig. 1 Optical and electronic arrangement of the setup for DLS experiments. The main beam path and the reference beam path are indicated by solid and dashed lines. The components are: Mirrors (M), lens (L), beam splitter (BS), lambda-half wave plates (λ/2), polarization beam splitters (PBS), neutral density filter (ND), linear grey filter (GF), apertures (A), photomultiplier tubes (PMT), and sample cell (SC) (Color figure online)

temperature control loop is realized with a Pt100 resistance probe placed in the wall of the cell close to a resistance heating. To measure T of the fluid, a second resistance probe is placed inside the cell material close to the fluid. p is measured with a calibrated pressure transducer with an absolute expanded uncertainty ($k=2$) of 0.015 MPa.

At the beginning of an experimental series, the complete sample cell system including reservoirs was evacuated using an oil-sealed vacuum pump to $p \approx 0.4$ Pa for 30 min. Thereafter, the entire system was filled with the gas mixture using a lubricant-free gas compressor and injection valves. In this way, the desired p in the sample cell could be adjusted. For each thermodynamic state, four individual measurements were performed at Θ_I between (2.3 and 3.0)°. T and p data reported in the tables and figures of Sect. 4 are average values obtained for individual measurements at different Θ_I lasting approximately 30 min. On average, the stability of T and p during the complete measurement series at a given thermodynamic state were ± 4 mK and $\pm 1 \times 10^{-2}$ MPa. For each individual measurement at defined Θ_I, the stabilities of T and p were less than ± 2 mK and $\pm 5 \times 10^{-3}$ MPa.

3.3 Data Evaluation and Interpretation

For binary mixtures of H_2 and CH_4 at $x_{CH_4} = (0.0533$ and $0.8319)$ and at T and p of about 333 K and 15 MPa, two examples of experimental CFs recorded by a linear-tau correlator are shown in the upper parts of Fig. 2(a) and (b). In the present work, only a single hydrodynamic mode was resolvable in the experimental CFs for all binary mixtures studied. For data evaluation, Eq. 2 is reduced to

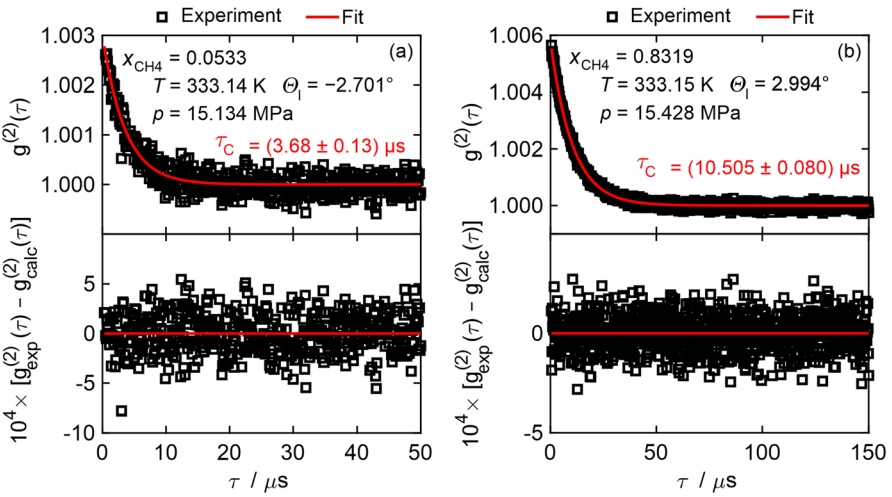

Fig. 2 Measured CFs and their fits (upper parts) and residuals of the measured data from the fits to CFs (lower parts) recorded by a linear-tau correlator for gaseous binary mixtures of H_2 and CH_4 at $x_{CH_4} = 0.0533$ (a) and 0.8319 (b) and at T and p of about 333 K and 15 MPa (Color figure online)

$$g^{(2)}(\tau) = b_0 + b \exp\left(-|\tau|/\tau_C\right) \tag{17}$$

and only a single characteristic decay time τ_C and amplitude b are obtained from the fit. For an accurate analysis, a linear term or a second-order polynomial was added to the theoretical fit model according to Eq. 17, if necessary. All CFs were fitted using the nonlinear Levenberg–Marquardt algorithm. The presence of a single hydrodynamic mode is confirmed by the residual plots in the lower parts of Fig. 2(a) and (b). Here, no systematic behaviors can be found.

Each diffusivity datum reported in Table 1 represents the average value obtained from eight independent experimental CFs recorded for at least four different Θ_I by using the linear- and multi-tau correlators. The averaging is performed by using a weighting scheme which considers the statistical uncertainty of the correlator data as well as the uncertainty of the measurement of Θ_I [31]. In general, smaller uncertainties are obtained in mixtures with larger ρ_{mix}, i.e., higher x_{CH_4} at similar T and p, which is directly reflected by the SNR of the experimental CFs, as can be seen in Fig. 2. The largest uncertainties are obtained for $x_{CH_4} = 0.0533$ at $p = 5$ MPa and $T = 373$ K.

Assuming that coupling between heat and mass transfer is absent, the single hydrodynamic mode observed in the DLS experiments might be interpreted as a mixed diffusivity D_m. However, as discussed in Sect. 2.1, depending on the values of Le and $\mathfrak{R}$, the determined diffusivity might rather be a or D_{11}. In the following, the obtained diffusivities are presented and they are assigned to a, D_{11}, or D_m by considering predicted and literature data for the diffusivities as well as the qualitative behavior of $\mathfrak{R}$.

4 Results and Discussion

The present experimental diffusivity data are shown in Fig. 3 by open diamonds as a function of x_{CH_4} at different T that are indicated by color. In Fig. 3, the parts (a), (b), and (c) correspond to $p \approx$ (5, 10, and 15) MPa. The expanded experimental uncertainties ($k = 2$) range from (0.91 to 14)%, are on average 3.8%, and are indicated by error bars if they are larger than the symbol size. The data shown at $x_{CH_4} = 1$ correspond to a of pure CH_4 determined in this work. In general, smaller diffusivities are obtained for larger p, and the diffusivities decrease with increasing x_{CH_4} and decreasing T for a given p.

For comparison and assignment of the experimentally determined diffusivities, also predicted and literature a and D_{11} data are shown in Fig. 3. The solid lines represent exponential fits of D_{11} predicted with the Chapman–Enskog theory [27] by calculating $[D_{11}]_2$ according to Eqs. 4–10 at the experimentally studied state points. Experimental D_{11} data for comparison can be found in the work of Bogatyrev and Nezovitina [24], who studied mixtures of H_2 and CH_4 at T and p between (250 and 900) K and (0.1 and 14) MPa using the steady-flow method. This method yields a composition-independent integral diffusion coefficient $D_{11,lit}$ that is most likely close to D_{11} at $x_{CH_4} = 0.5$. Since the exact composition is not known, the corresponding T- and p-interpolated D_{11} data are indicated by horizontal dashed lines in Fig. 3. The

Table 1 Thermal diffusivity a, Fick diffusion coefficient D_{11}, or mixed diffusivity D_m together with their relative expanded ($k = 2$) uncertainties U_r obtained for mixtures of H_2 and CH_4 or pure CH_4 by DLS as a function of temperature T and pressure p at different CH_4 mole fractions x_{CH_4} given in the respective header of the dataset.[a,b]

T/K	p/MPa	$10^6 \times D_{11}/(m^2 \cdot s^{-1})$	$100 \times U_r(D_{11})$
0.0533 CH_4 + 0.9467 H_2			
293.12	5.029	2.03	7.4
293.12	10.081	0.988	4.6
293.11	15.149	0.675	5.3
333.14	5.004	2.38	6.3
333.14	10.099	1.25	8.1
333.13	15.116	0.843	5.9
363.13	5.026	2.721	1.3
363.15	10.045	1.363	7.2
363.15	15.049	0.956	6.7
393.12	5.014	3.02	14
393.14	10.287	1.49	9.6
393.14	15.236	1.10	10
T/K	p/MPa	$10^6 \times D_m/(m^2 \cdot s^{-1})$	$100 \times U_r(D_m)$
0.3125 CH_4 + 0.6874 H_2			
293.13	5.005	1.382	3.1
293.13	10.018	0.651	2.4
293.12	15.039	0.416	5.6
333.15	5.033	1.70	8.8
333.15	10.020	0.831	1.8
333.16	15.065	0.5406	1.7
363.14	5.033	2.09	6.2
363.14	10.028	0.962	5.1
363.14	15.085	0.654	3.7
393.08	5.000	2.46	6.3
393.05	10.044	1.129	4.5
393.13	15.090	0.746	2.2
T/K	p/MPa	$10^6 \times a/(m^2 \cdot s^{-1})$	$100 \times U_r(a)$
0.6180 CH_4 + 0.3820 H_2			
293.13	5.026	0.938	2.2
293.12	10.082	0.422	2.7
293.12	15.157	0.2594	2.2
333.15	5.015	1.184	4.0
333.17	10.011	0.575	5.1
333.16	15.282	0.355	2.9
363.14	5.004	1.434	5.1
363.13	10.052	0.694	1.5
363.15	15.021	0.441	4.2

Table 1 (continued)

T/K	p/MPa	$10^6 \times a/(m^2 \cdot s^{-1})$	$100 \times U_r(a)$
393.06	5.030	1.593	5.0
393.03	10.061	0.792	2.4
393.03	15.259	0.5130	1.8
0.8319 CH_4 + 0.1681 H_2			
293.12	5.001	0.612	2.7
293.11	10.051	0.2766	2.3
293.11	15.236	0.1725	1.1
333.13	5.043	0.806	5.8
333.14	10.083	0.384	2.9
333.16	15.423	0.2482	1.9
363.14	5.092	0.938	2.1
363.10	10.082	0.4753	1.8
363.09	15.262	0.3095	2.4
393.02	5.001	1.119	2.9
393.01	9.978	0.567	3.1
393.13	15.132	0.3704	2.5
Pure CH_4			
293.11	5.067	0.4013	1.1
293.13	10.104	0.1834	1.7
293.14	15.077	0.1233	2.9
333.16	5.065	0.543	2.2
333.13	10.058	0.2647	2.1
333.13	15.312	0.1749	0.91
363.12	5.067	0.638	1.7
363.09	10.011	0.3200	1.0
363.14	15.130	0.2192	1.7
393.09	5.082	0.752	2.2
393.07	10.076	0.3766	1.8
393.14	14.935	0.2630	1.8

[a]Expanded uncertainties for T and p are $U(T) = 0.015$ K and $U(p) = 0.015$ MPa ($k = 2$). The relative expanded uncertainties $U_r(a)$, $U_r(D_{11})$, and $U_r(D_m)$ for all individual a, D_{11}, and D_m values, respectively, are given in the table ($k = 2$)

[b]Expanded absolute uncertainty for x_{CH_4} stated by the supplier is $U(x_{CH_4}) = 0.01$

dotted lines in Fig. 3 represent the predicted thermal diffusivity data a_{mix} calculated with the model from Lima et al. [47] as a function of x_{CH_4} according to Eqs. 11–13. The lines composed of x symbols correspond to the thermal diffusivity obtained by using Eq. 14 and literature data [49–54], $a_{mix,REFPROP}$, which is always larger than a_{mix}. While good agreement between a_{mix} and $a_{mix,REFPROP}$ is observed for x_{CH_4} close to 0 or 1, deviations of up to 27% are observed for about $0.1 < x_{CH_4} < 0.8$. Here, particularly large discrepancies are observed at low T and high p. This can be seen from

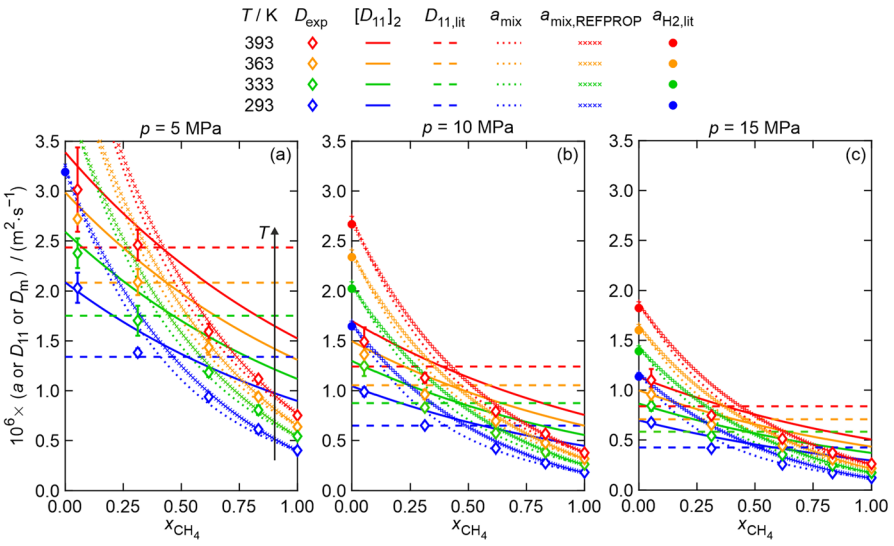

Fig. 3 Thermal diffusivity a, Fick diffusion coefficient D_{11}, or mixed diffusivity D_m in the gaseous phase of mixtures of H_2 and CH_4 or pure CH_4 obtained by DLS (D_{exp}, diamonds) as a function of the CH_4 mole fraction x_{CH_4} at $T=293$ K (blue), $T=333$ K (green), $T=363$ K (orange), and $T=393$ K (red). (a), (b), and (c) show the results for $p=(5, 10,$ and $15)$ MPa. Expanded uncertainties ($k=2$) of the present experimental data are shown as error bars if they are larger than the symbol size. The solid and dotted lines represent predicted D_{11} or a data by using the Chapman–Enskog theory [27], $[D_{11}]_2$, or the model proposed by Lima et al. [47], a_{mix}. Data for the composition-independent integral diffusion coefficient $D_{11,lit}$ from Bogatyrev and Nezovitina [26] interpolated to the present T and p is indicated by dashed lines. a data for the mixtures from Eq. 14 by using literature data [49–54], $a_{mix,REFPROP}$, or for pure H_2 obtained via $a_{H2,lit}=\lambda\cdot\rho^{-1}\cdot c_p^{-1}$ by using data reported in a data compilation [62] is indicated by lines composed of x symbols or filled circles (Color figure online)

the deviation plots shown in Fig. 4. In addition, thermal diffusivity data of pure H_2, $a_{H2,lit}$, calculated in the same way as $a_{mix,REFPROP}$ by Eq. 14 using ρ, c_p, and λ data of pure H_2 reported in a data compilation [62] is shown in Fig. 3 by filled circles at $x_{CH_4}=0$. Here, as expected, good agreement between $a_{H_2,lit}$, a_{mix}, and $a_{mix,REFPROP}$ is observed.

Besides serving for the intended use for the assignment of the experimentally obtained diffusivities, the predicted and literature a and D_{11} data indicate that the magnitudes of a and D_{11} are quite similar at a given thermodynamic state and that for each T and p, there is a x_{CH_4} where Le equals one, cf. Figure 3.

As it can be seen from Fig. 3 as well as from the deviation plots in Figs. 4 and 5, at the lowest x_{CH_4} studied, i.e., at $x_{CH_4}=0.0533$, the present diffusivity data agree within experimental uncertainties with the $[D_{11}]_2$ values predicted by the Chapman–Enskog theory, whereas large deviations from the predicted a_{mix}, $a_{mix,REFPROP}$, and $a_{H2,lit}$ are observed. Therefore, for all T and p investigated at $x_{CH_4}=0.0533$, the obtained diffusivity is attributed to D_{11}. The diffusivities determined at $x_{CH_4}=0.3125$ appear to be in agreement with the integral diffusion coefficient data from Bogatyrev and Nezovitina [26] for most of the thermodynamic states investigated, but not with

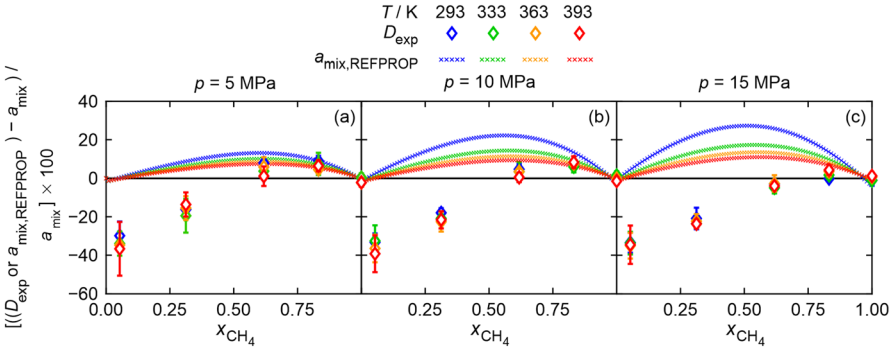

Fig. 4 Relative deviations of the diffusivities obtained by DLS (D_{exp}, diamonds) or the thermal diffusivity obtained from Eq. 14 by using literature data [49–54] ($a_{mix,REFPROP}$, lines composed of x symbols) in the gaseous phase of mixtures of H_2 and CH_4 or pure CH_4 from a_{mix} calculated by Eqs. 11–13 as a function of the CH_4 mole fraction x_{CH_4} at $T=293$ K (blue), $T=333$ K (green), $T=363$ K (orange), and $T=393$ K (red). (a), (b), and (c) show the results for $p=(5,$ 10, and 15) MPa. Expanded uncertainties ($k=2$) of the present experimental data are shown as error bars if they are larger than the symbol size (Color figure online)

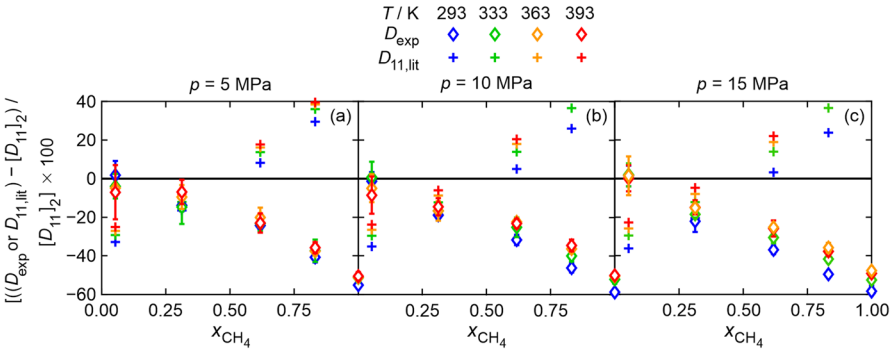

Fig. 5 Relative deviations of the diffusivities obtained by DLS (D_{exp}, diamonds) or the integral diffusion coefficient data from Bogatyrev and Nezovitina [26] ($D_{11,lit}$, + symbols) in the gaseous phase of mixtures of H_2 and CH_4 or pure CH_4 from $[D_{11}]_2$ calculated by Eqs. 4–10 as a function of the CH_4 mole fraction x_{CH_4} at $T=293$ K (blue), $T=333$ K (green), $T=363$ K (orange), and $T=393$ K (red). (a), (b), and (c) show the results for $p=(5,$ 10, and 15) MPa. Expanded uncertainties ($k=2$) of the present experimental data are shown as error bars if they are larger than the symbol size (Color figure online)

a_{mix}, $a_{mix,REFPROP}$, or $[D_{11}]_2$, which are always larger. Such behavior is unexpected and difficult to explain, since D_m should lie between a and D_{11} at a given state point. Since no better assignment is possible based on the available literature and predicted data, these diffusivities are attributed to D_m. Except for $T=393$ K, the data from Bogatyrev and Nezovitina [26] show relatively good agreement with $[D_{11}]_2$ at $x_{CH_4}=0.5$, which can be interpreted as validation of the experimental data from Ref. [26]. For $x_{CH_4}=(0.6180$ and $0.8319)$, the present diffusivity data show large deviations from $[D_{11}]_2$ and agree with the a_{mix} and $a_{mix,REFPROP}$ data. Therefore, these experimental data are attributed to a. This is supported by the trend of the

experimental diffusivities toward $x_{CH_4}=1$, where agreement is found between the present a data of pure CH_4, a_{mix}, and $a_{mix,REFPROP}$.

A closer look at the deviations between a, a_{mix}, and $a_{mix,REFPROP}$ for $x_{CH_4}=(0.6180$ and $0.8319)$, visible in Fig. 4, reveals that for $p=5$ MPa, a is always between a_{mix} and $a_{mix,REFPROP}$, but closer to $a_{mix,REFPROP}$ for $x_{CH_4}=0.8319$. At $p=(10$ and $15)$ MPa and all T, better agreement is found between a and a_{mix}. Consequently, Eq. 14 in connection with literature data [49–54] appears to be more reliable for predicting a at low p and the Lima et al. [47] model for predicting a at high p for $x_{CH_4}<0.95$. No significant differences between a_{mix} and $a_{mix,REFPROP}$ are observed for $x_{CH_4}>0.95$. Thus, both Eq. 14 [49–54] and the model from Lima et al. [47] can be used to predict a for these x_{CH_4}.

The assignment of the diffusivities measured by DLS to D_{11} at low x_{CH_4} and to a at large x_{CH_4} is supported by the calculated $\mathfrak{R}$ values. Here, for each T and p, decreasing $\mathfrak{R}$ values were found with increasing x_{CH_4}. This indicates that with increasing x_{CH_4}, the signal related to fluctuations in concentration becomes weaker relative to the signal related to fluctuations in T. Further interpretation based on $\mathfrak{R}$ cannot be performed due to the difficulties in connection with the calculation of $(\partial c/\partial\mu)$ as detailed earlier.

The attributed diffusivity data together with their respective expanded uncertainties $(k=2)$ are summarized in Table 1. It should be noted that the uncertainty reported for D_m only quantifies how accurately the diffusivity could be determined by DLS, but not how well it matches a and/or D_{11}.

The application of the Chapman–Enskog theory [27] for the calculation of $[D_{11}]_2$ is quite cumbersome and predicting a_{mix} with the model from Lima et al. [47] requires pure substance data. This motivated the development of simple correlations for the description of D_{11} or a in gaseous mixtures of H_2 and CH_4 as a function of T, p, and x_{CH_4} in the studied range. The correlation is given by

$$D_{11,calc}, a_{calc} = \frac{1}{b_0 p}\exp\left(b_1 T + b_2 x_{CH_4}^{b_3} - x_{CH_4}\right), \tag{18}$$

where T is the temperature in K, p the pressure in MPa, x_{CH_4} the mole fraction of CH_4, and $D_{11,calc}$ or a_{calc} the calculated diffusivity in $m^2{\cdot}s^{-1}$. For $D_{11,calc}$, the parameters b_0, b_1, b_2, and b_3 reported in Table 2 were obtained by non-linear regression of $[D_{11}]_2$ calculated via Eqs. 4–10. To obtain the parameters for a_{calc}, a_{mix} and $a_{mix,REFPROP}$ calculated by Eqs. 11–13 and Eq. 14 as well as the experimental diffusivity data that were assigned to a were considered. Details about the data used

Table 2 Coefficients of Eq. 18

Parameter	Equation 18 Fick diffusivity $D_{11,calc}$	Equation 18 thermal diffusivity a_{calc}
$b_0/(s{\cdot}m^{-2}{\cdot}MPa^{-1})$	4.08×10^5	3.55×10^5
b_1/K^{-1}	5.03×10^{-3}	5.85×10^{-3}
b_2	0.179	−1.004
b_3	1.753	1.007

for fitting are given in the Supporting Information. By using Eq. 18 and the parameters given in Table 2, a maximum absolute relative deviation (MARD) of 2.9% and an average absolute relative deviation (AARD) of 0.98% of $D_{11,\mathrm{calc}}$ from the $[D_{11}]_2$ training data set are observed. For a_{calc}, a MARD of 15% and an AARD of 4.6% of a_{calc} from the training data set containing a_{mix} and $a_{\mathrm{mix,REFPROP}}$ are obtained. The larger deviations observed for the correlation of a data are due to the discrepancies between both training data sets as described above. Except for D_{11} at $T=363.15$ K, $p=5.062$ MPa, and $x_{\mathrm{CH_4}}=0.0533$, the correlation given by Eq. 18 can predict the present experimental D_{11} data within the experimental uncertainties. For the experimental a data obtained in this work, an AARD of 4.4% of a from Eq. 18 is observed, which is smaller than the AARD of the training set.

For further validation of the correlation, comparison with literature D_{11} data from Gotoh et al. [28] was performed. These authors investigated an equimolar mixture of H_2 and CH_4 at $p=1$ atm and $T=(298.0, 378.3, \text{and } 438.4)$ K with the Loschmidt method. Here, relative deviations of $(-7.7, -6.4, \text{and} -2.0)$% from Eq. 18 are observed.

5 Conclusion

Gaseous mixtures of H_2 and CH_4 were studied by DLS experiments at T between (293 and 393) K, p between (5 and 15) MPa, and $x_{\mathrm{CH_4}}$ between (0.05 and 1). For each thermodynamic state investigated, only one hydrodynamic mode was observable in the experimental correlation functions. The related diffusivity shows a decreasing trend with decreasing T and increasing p and $x_{\mathrm{CH_4}}$. Corresponding expanded ($k=2$) experimental uncertainties range from (0.91 to 14)% and are on average 3.8%. Comparison of the present diffusivity results with predicted and literature diffusivity data as well as with the qualitative behavior of the estimated Rayleigh ratio allowed assignment of the obtained diffusivities to the Fick diffusion coefficient D_{11} at $x_{\mathrm{CH_4}}=0.0533$, a mixed diffusivity D_{m} representing both a and D_{11} at $x_{\mathrm{CH_4}}=0.3125$, and the thermal diffusivity a at $x_{\mathrm{CH_4}}=(0.6180 \text{ and } 0.8319)$. Based on the understanding gained and data measured or calculated in this study, correlations for D_{11} and a were established, which give access to both diffusivities in gaseous mixtures of H_2 and CH_4 as a function of T, p, and $x_{\mathrm{CH_4}}$. Considering the remaining difficulties in assigning the single hydrodynamic mode observed in gaseous mixtures by DLS, further experimental and theoretical work is desirable to improve the general understanding.

Supplementary Information The online version contains supplementary material available at https://doi.org/10.1007/s10765-023-03250-x.

Acknowledgements The authors gratefully acknowledge funding of the Erlangen Graduate School in Advanced Optical Technologies (SAOT) by the Bavarian State Ministry for Science and Art.

Author Contributions MP measured the diffusivities and wrote the main manuscript text. PS supported the measurements of diffusivities. All authors reviewed the manuscript.

Funding Open Access funding enabled and organized by Projekt DEAL. This work was supported by Shell Global Solutions International BV through a contracted research agreement.

Data Availability Not applicable.

Declarations

Competing Interests The authors declare they have no competing interests as defined by Springer, or other interests that might be perceived to influence the results and/or discussion reported in this paper.

References

1. A. Kovač, M. Paranos, D. Marciuš, Int. J. Hydrogen Energy **46**, 10016 (2021). https://doi.org/10.1016/j.ijhydene.2020.11.256
2. A.M. Abdalla, S. Hossain, O.B. Nisfindy, A.T. Azad, M. Dawood, A.K. Azad, Energy Convers. Manag. **165**, 602 (2018). https://doi.org/10.1016/j.enconman.2018.03.088
3. S.E. Hosseini, M.A. Wahid, Int. J. Energy Res. **44**, 4110 (2020). https://doi.org/10.1002/er.4930
4. C. Acar, I. Dincer, J. Clean. Prod. **218**, 835 (2019). https://doi.org/10.1016/j.jclepro.2019.02.046
5. H. Ishaq, I. Dincer, Renew. Sustain. Energy Rev. **135**, 110192 (2021). https://doi.org/10.1016/j.rser.2020.110192
6. S.E. Hosseini, M.A. Wahid, Renew. Sustain. Energy Rev. **57**, 850 (2016). https://doi.org/10.1016/j.rser.2015.12.112
7. J. Kurtz, S. Sprik, T.H. Bradley, Int. J. Hydrogen Energy **44**, 12010 (2019). https://doi.org/10.1016/j.ijhydene.2019.03.027
8. M.R. Usman, Renew. Sustain. Energy Rev. **167**, 112743 (2022). https://doi.org/10.1016/j.rser.2022.112743
9. D. Zivar, S. Kumar, J. Foroozesh, Int. J. Hydrogen Energy **46**, 23436 (2021). https://doi.org/10.1016/j.ijhydene.2020.08.138
10. L. García, in *Woodhead Publ. Ser. Energy*, ed. by V. Subramani, A. Basile, and T.N. Veziroğlu (Woodhead Publishing, Oxford, 2015), pp. 83–107. https://doi.org/10.1016/B978-1-78242-361-4.00004-2
11. N. Sánchez-Bastardo, R. Schlögl, H. Ruland, Ind. Eng. Chem. Res. **60**, 11855 (2021). https://doi.org/10.1021/acs.iecr.1c01679
12. G. Iervolino, V. Vaiano, J.J. Murcia, A.E. Lara, J.S. Hernández, H. Rojas, J.A. Navío, M.C. Hidalgo, Int. J. Hydrogen Energy **46**, 38678 (2021). https://doi.org/10.1016/j.ijhydene.2021.09.111
13. D. Haeseldonckx, W. D'haeseleer, Int. J. Hydrogen Energy **32**, 1381 (2007). https://doi.org/10.1016/j.ijhydene.2006.10.018
14. Q. Xue, M. Wu, X.C. Zeng, P. Jena, J. Mater. Chem. A **6**, 8916 (2018). https://doi.org/10.1039/C8TA01909F
15. S. Moon, Y. Lee, D. Seo, S. Lee, S. Hong, Y.-H. Ahn, Y. Park, Renew. Sustain. Energy Rev. **141**, 110789 (2021). https://doi.org/10.1016/j.rser.2021.110789
16. E.I. Epelle, W. Obande, G.A. Udourioh, I.C. Afolabi, K.S. Desongu, U. Orivri, B. Gunes, J.A. Okolie, Sustain. Energy Fuels **6**, 3324 (2022). https://doi.org/10.1039/D2SE00618A

17. N.S. Muhammed, M.B. Haq, D.A. Al Shehri, A. Al-Ahmed, M.M. Rahman, E. Zaman, S. Iglauer, Fuel **337**, 127032 (2023). https://doi.org/10.1016/j.fuel.2022.127032
18. M. Zamehrian, B. Sedaee, J. Pet. Sci. Eng. **212**, 110304 (2022). https://doi.org/10.1016/j.petrol.2022.110304
19. M. Kanaani, B. Sedaee, M. Asadian-Pakfar, J. Energy Storage **45**, 103783 (2022). https://doi.org/10.1016/j.est.2021.103783
20. M. Richter, M.A. Ben Souissi, R. Span, P. Schley, J. Chem. Eng. Data **59**, 2021 (2014). https://doi.org/10.1021/je500181v
21. R. Beckmüller, M. Thol, I.H. Bell, E.W. Lemmon, R. Span, J. Phys. Chem. Ref. Data **50**, 13102 (2021). https://doi.org/10.1063/5.0040533
22. R. Amaduzzi, M. Ferrarotti, A. Parente, Front. Energy Res. **8** (2021). https://doi.org/10.3389/fenrg.2020.590300
23. A. Witkowski, A. Rusin, M. Majkut, K. Stolecka, Int. J. Press. Vessel. Pip. **166**, 24 (2018). https://doi.org/10.1016/j.ijpvp.2018.08.002
24. S. Di Iorio, P. Sementa, B.M. Vaglieco, Int. J. Hydrogen Energy **39**, 9809 (2014). https://doi.org/10.1016/j.energy.2015.02.051
25. Y. Kobayashi, A. Kurokawa, M. Hirata, J. Therm. Sci. Technol. **2**, 236 (2007). https://doi.org/10.1299/jtst.2.236
26. A.F. Bogatyrev, M.A. Nezovitina, Int. J. Thermophys. **34**, 2065 (2013). https://doi.org/10.1007/s10765-013-1539-3
27. T.R. Marrero, E.A. Mason, J. Phys. Chem. Ref. Data **1**, 3 (1972). https://doi.org/10.1063/1.3253094
28. S. Gotoh, M. Manner, J.P. Sorensen, W.E. Stewart, J. Chem. Eng. Data **19**, 169 (1974). https://doi.org/10.1021/je60061a025
29. L.R. Fokin, A.N. Kalashnikov, A.F. Zolotukhina, J. Eng. Phys. Thermophys. **84**, 1408 (2011). https://doi.org/10.1007/s10891-011-0612-7
30. A. Heller, M.H. Rausch, P.S. Schulz, P. Wasserscheid, A.P. Fröba, J. Chem. Eng. Data **61**, 504 (2016). https://doi.org/10.1021/acs.jced.5b00671
31. M. Piszko, W. Wu, S. Will, M.H. Rausch, C. Giraudet, A.P. Fröba, Fuel **242**, 562 (2019). https://doi.org/10.1016/j.fuel.2019.01.078
32. M. Piszko, F.D. Lenahan, L. Friedl, T. Klein, A.P. Fröba, J. Chem. Eng. Data **67**, 3059 (2022). https://doi.org/10.1021/acs.jced.2c00487
33. B.J. Berne, R. Pecora, *Dynamic Light Scattering: With Applications to Chemistry, Biology, and Physics* (Dover Publ Courier Corporation, Mineola, 2000)
34. A.P. Fröba, Dynamic Light Scattering (DLS) for the Characterization of Working Fluids in Chemical and Energy Engineering, Friedrich-Alexander-Universität, Habil. Thesis, 2009.
35. M. Piszko, K. Batz, M.H. Rausch, C. Giraudet, A.P. Fröba, J. Chem. Eng. Data **65**, 1068 (2019). https://doi.org/10.1021/acs.jced.9b00495
36. M. Piszko, C. Giraudet, A.P. Fröba, Int. J. Thermophys. **41**, 1 (2020). https://doi.org/10.1007/s10765-020-02680-1
37. A.P. Fröba, A. Leipertz, Diffus. Fundam. **2**, 1 (2005)
38. J.P. Boon, S. Yip, *Molecular Hydrodynamics* (Dover Publ Courier Corporation, Mineola, 1980)
39. J.M. Ortiz de Zárate, J.V. Sengers, *Hydrodynamic Fluctuations* (Elsevier, Amsterdam, 2006)
40. A.P. Fröba, S. Will, A. Leipertz, Int. J. Thermophys. **21**, 603 (2000). https://doi.org/10.1023/A:1006629516889
41. P.N. Segrè, J.V. Sengers, Physica A **198**, 46 (1993). https://doi.org/10.1016/0378-4371(93)90183-5
42. M.A. Anisimov, V.A. Agayan, A.A. Povodyrev, J.V. Sengers, E.E. Gorodetskii, Phys. Rev. E **57**, 1946 (1998). https://doi.org/10.1103/PhysRevE.57.1946
43. A.F. Bogatyrev, V.R. Belalov, M.A. Nezovitina, J. Eng. Phys. Thermophys. **86**, 1225 (2013). https://doi.org/10.1007/s10891-013-0945-5
44. S. Chapman, T.G. Cowling, D. Burnett, C. Cercignani, *The Mathematical Theory of Non-Uniform Gases: An Account of the Kinetic Theory of Viscosity, Thermal Conduction and Diffusion in Gases* (Cambridge University Press, Cambridge, 1990)
45. M. Klein, F.J. Smith, J. Res. Natl. Bur. Stand. A **72A**, 359 (1968)
46. L.D. Smoot, D.T. Pratt, *Pulverized-Coal Combustion and Gasification*, 1st edn. (Springer, New York, 1979). https://doi.org/10.6028/jres.072A.033
47. J.A.P. Lima, E. Marín, M.G. da Silva, M.S. Sthel, S.L. Cardoso, H. Vargas, L.C.M. Miranda, Rev. Sci. Instrum. **72**, 1580 (2001). https://doi.org/10.1063/1.1334622

48. J.A.P. Lima, E. Marín, M.G. da Silva, M.S. Sthel, D.U. Schramm, S.L. Cardoso, H. Vargas, L.C.M. Miranda, Meas. Sci. Technol. **12**, 1949 (2001). https://doi.org/10.1088/0957-0233/12/11/326
49. J.W. Leachman, R.T. Jacobsen, S.G. Penoncello, E.W. Lemmon, J. Phys. Chem. Ref. Data **38**, 721 (2009). https://doi.org/10.1063/1.3160306
50. M.J. Assael, J.-A.M. Assael, M.L. Huber, R.A. Perkins, Y. Takata, J. Phys. Chem. Ref. Data **40**, 33101 (2011). https://doi.org/10.1063/1.3606499
51. U. Setzmann, W. Wagner, J. Phys. Chem. Ref. Data **20**, 1061 (1991). https://doi.org/10.1063/1.555898
52. D.G. Friend, J.F. Ely, H. Ingham, *Tables for the Thermophysical Properties of Methane* (NIST Technical Note 1325, 1989)
53. O. Kunz, R. Klimeck, W. Wagner, M. Jaeschke, *The GERG-2004 Wide-Range Equation of State for Natural Gases and Other Mixtures* (VDI Verlag GmbH, Düsseldorf, 2007)
54. O. Kunz, W. Wagner, J. Chem. Eng. Data **57**, 3032 (2012). https://doi.org/10.1021/je300655b
55. E.W. Lemmon, I.H. Bell, M.L. Huber, M.O. McLinden, REFPROP, Standard Reference Data Program. Version 10.0. (NIST, Gaithersburg, 2018). https://doi.org/10.18434/T4/1502528
56. H.A. Lorentz, *The Theory of Electrons and Its Applications to the Phenomena of Light and Radiant Heat*, 2nd edn. (B.G. Teubner, Leipzig, 1916)
57. W.B. Li, R.W.G. Segré, J.V. Sengers, M. Lamvik, J. Chem. Phys. **101**, 5058 (1994). https://doi.org/10.1063/1.467428
58. M. Gebhardt, W. Köhler, A. Mialdun, V. Yasnou, V. Shevtsova, J. Chem. Phys. **138**, 114503 (2013). https://doi.org/10.1063/1.4795432
59. C. Giraudet, L. Marlin, D. Bégué, F. Croccolo, H. Bataller, J. Chem. Phys. **144**, 134304 (2016). https://doi.org/10.1063/1.4944984
60. T.N. Olney, N.M. Cann, G. Cooper, C.E. Brion, Chem. Phys. **223**, 59 (1997). https://doi.org/10.1016/S0301-0104(97)00145-6
61. M. DuBois, P. Berge, Phys. Rev. Lett. **26**, 121 (1971). https://doi.org/10.1103/PhysRevLett.26.121
62. R.D. McCarty, J. Hord, H.M. Roder, *Selected Properties of Hydrogen (Engineering Design Data)* (National Engineering Lab (NBS), Boulder, 1981)